iScience

CellPress
OPEN ACCESS

Article

Large-scale survey of excitatory synapses reveals sublamina-specific and asymmetric synapse disassembly in a neurodegenerative circuit

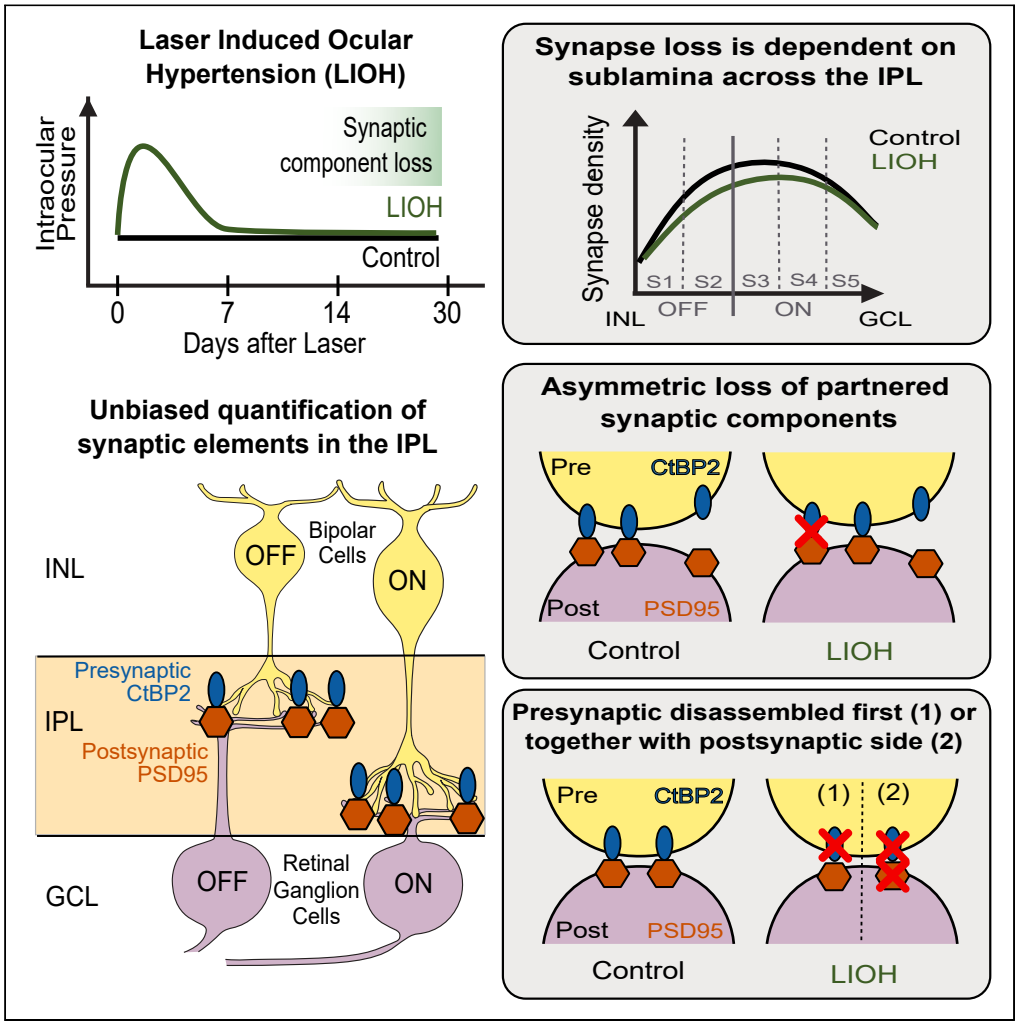

Manuel Soliño, Alfred Yu, Luca Della Santina, Yvonne Ou

ldellasantina@uh.edu (L.D.S.)
yvonne.ou@ucsf.edu (Y.O.)

Highlights

Pre- and postsynaptic component loss occurs across the IPL after IOP elevation

The susceptibility of pre- versus postsynaptic components is sublamina-dependent

Partnered synaptic component loss is asymmetric between pre- and postsynaptic sites

Presynaptic component loss precedes or coincides with postsynaptic component loss

Soliño et al., iScience 26, 107262
August 18, 2023
https://doi.org/10.1016/j.isci.2023.107262

iScience

CellPress
OPEN ACCESS

Article

Large-scale survey of excitatory synapses reveals sublamina-specific and asymmetric synapse disassembly in a neurodegenerative circuit

Manuel Soliño,[1] Alfred Yu,[1] Luca Della Santina,[1,2,3,*] and Yvonne Ou[1,3,4,*]

SUMMARY

In the nervous system, parallel circuits are organized in part by the lamina-specific compartmentalization of synaptic connections. In sensory systems such as mammalian retina, degenerating third-order neurons remodel their local presynaptic connectivity with second-order neurons. To determine whether there are sublamina-specific perturbations after injury of adult retinal ganglion cells, we comprehensively analyzed excitatory synapses across the inner plexiform layer (IPL) where bipolar cells connect to ganglion cells. Here, we show that pre- and postsynaptic component loss occurs throughout the IPL in a sublamina-dependent fashion after transient intraocular pressure elevation. Partnered synaptic components are lost as neurodegeneration progresses, while unpartnered synaptic components remain stable. Furthermore, presynaptic components are either lost first or simultaneously with the postsynaptic component. Our results demonstrate that this degenerating neural circuit exhibits differential vulnerability of excitatory synapses depending on IPL depth, highlighting the ordered disassembly of synapses that is specific to laminar compartments of the retina.

INTRODUCTION

In the nervous system, the lamina-specific compartmentalization of synaptic connections that underlies many CNS circuits is important for parallel processing of neural information. During development, circuit remodeling is a critical step toward refining neuronal connectivity and ensuring proper function, and involves both synapse assembly and disassembly.[1–3] The adult vertebrate retina is a well-studied example of a laminated tissue in the CNS, in which synaptic connections between specific neurons are compartmentalized in two major layers, the inner plexiform layer (IPL) and outer plexiform layer (OPL). Activity-dependent and activity-independent mechanisms act in concert to establish specific sublaminae in the inner retina.[4] However, while high fidelity circuit function is reliant on stereotyped patterns of synaptic connectivity among appropriately partnered neurons, the patterns and principles governing synapse disassembly during neurodegeneration are not well understood.[5]

Glaucoma is a neurodegenerative disease in which synapse disassembly is an early event after the postsynaptic neuron, the retinal ganglion cell (RGC), is injured. In experimental glaucoma models, postsynaptic components are disassembled without retraction of the axon terminals of presynaptic partners.[6,7] However, at the individual RGC level, we recently demonstrated that presynaptic ribbons are disassembled before postsynaptic scaffolding proteins in $A_{ON\text{-}Sustained}$ RGCs.[7] Furthermore, presynaptic ribbons and RGCs whose dendrites stratify in the OFF sublamina of the inner plexiform layer (IPL) appear to be more vulnerable to intraocular pressure (IOP) elevation, the only modifiable risk factor in glaucoma.[8–13] For example, $A_{OFF\text{-}Transient}$ RGCs have been identified as more susceptible to elevated IOP, whereas $A_{ON\text{-}Sustained}$ RGCs are more resilient, and even exhibit rewiring with former developmental partners, rod bipolar cells.[7] However, others have identified alternative patterns of RGC type susceptibility that do not follow ON versus OFF polarity.[14–21] Furthermore, it is not known whether these principles of synapse disassembly when RGCs degenerate are generalizable across the sublamina of the IPL.

Although single cell analyses have supported the notion that RGCs and synapses in the OFF sublamina are more vulnerable than those in the ON sublamina,[7,12] here we significantly expand our view to assess whether these principles are applicable across neurons and the entire IPL. We used a laser-induced ocular

[1]Department of Ophthalmology, University of California San Francisco School of Medicine, San Francisco, CA 94143, USA

[2]College of Optometry, University of Houston, Houston, TX 77204, USA

[3]Senior authors

[4]Lead contact

*Correspondence: ldellasantina@uh.edu (L.D.S.), yvonne.ou@ucsf.edu (Y.O.)

https://doi.org/10.1016/j.isci.2023.107262

hypertension (LIOH) model in adult mice to transiently elevate IOP, and then quantified all excitatory synapses in the IPL across a volume of retina. Pre- and postsynaptic component loss is evident throughout the IPL, with differential susceptibility of synaptic components depending on IPL depth. As neurodegeneration progress, unpartnered puncta (defined as missing presynaptic or postsynaptic component) are stable while partnered puncta (defined as having colocalized presynaptic and postsynaptic components) are lost. Furthermore, presynaptic components are either lost first or simultaneously with the postsynaptic component. Together, these experiments suggest that injury to the postsynaptic neuron results in precise disassembly of synaptic connectivity and differential impairment of distinct functional microcircuits in the nervous system.

RESULTS

To examine synapse disassembly in a circuit in which the postsynaptic neuron is injured, we used the laser-induced ocular hypertension model which results in transient IOP elevation in the lasered eyes[7,12,22,23] (Figures 1A and 1B). Peak IOP occurs 24 h after the laser procedure, with return to baseline 5 days after treatment. The IOP integral is increased in the lasered eyes (26.5 $\pm$ 5.5 mmHg $\times$ day) versus control eyes (19.1 $\pm$ 2.7 mmHg $\times$ day) ($p < 0.0001$). We examined synapse disassembly at three time points: 7, 14, and 30 days. This model results in selective death of RGCs starting 14 days after the laser (Figures 1B and 1C), while IPL volume is not affected at any time point (Figure 1D).

IOP elevation results in loss of pre- and postsynaptic components throughout the inner retina

Our previous work demonstrates that both presynaptic ribbons found in BC axon terminals labeled by CtBP2 and postsynaptic density proteins (PSD95) on individually labeled alpha RGCs are lost after transient IOP elevation.[7,12] However, it is not known whether this finding is applicable across all RGC types. To automate the quantification of synapse density across the entire IPL, we first immunolabeled the presynaptic ribbon protein CtBP2 and the excitatory postsynaptic scaffolding protein PSD95, then identified and quantified all excitatory synapses in an IPL volume using ObjectFinder (Figures 1E–1G and STAR methods).

Starting at 14 days after laser-induced ocular hypertension, average PSD95 density decreased significantly compared to control eyes (0.20 $\pm$ 0.02 versus 0.22 $\pm$ 0.03 puncta/um^3, $p = 0.03$), whereas average CtBP2 density did not drop until 30 days after IOP elevation (0.16 $\pm$ 0.04 versus 0.18 $\pm$ 0.03 puncta/um3, $p = 0.005$) (Figures 1H and 1I). To understand whether partnered synaptic components (defined as colocalization of presynaptic CtBP2 and postsynaptic PSD95 puncta) (Figure 1J) are lost after IOP elevation, we quantified partnered puncta with CtBP2 or PSD95 as the reference object. No matter if the reference object was CtBP2 or PSD95, partnered synaptic components decreased starting at 14 days after IOP elevation when compared to control (CtBP2 colocalized with PSD95: 0.12 $\pm$ 0.02 versus 0.13 $\pm$ 0.02 puncta/um^3, $p = 0.002$; PSD95 colocalized with CtBP2: 0.12 $\pm$ 0.02 versus 0.14 $\pm$ 0.02, $p = 0.0008$; Figures 1M and N). Another metric with which to assess synapse disassembly is nearest neighbor distance, with the distance between components increasing as synapses are disassembled. The nearest neighbor distance between CtBP2 and PSD95 synaptic puncta increased at 30 days after IOP elevation irrespective of whether CtBP2 or PSD95 was used as the reference object, consistent with synapse disassembly over time (CtBP2 to PSD95: 0.64 $\pm$ 0.04 versus 0.69 $\pm$ 0.07 μm, $p = 0.005$; PSD95 to CtBP2: 0.98 $\pm$ 0.39 versus 0.77 $\pm$ 0.08 μm, $p = 0.01$, Figures 1K and L). In summary, these data reveal that when all excitatory synapses are quantified in a volume of IPL, pre- and postsynaptic component loss is apparent starting 14 days after IOP elevation.

The pattern of synaptic component loss is sublamina-specific

As we have previously shown that presynaptic ribbons are differentially lost across the ON versus OFF sublamina of a small volume of IPL,[12] we asked whether all excitatory synapses across an IPL volume are disassembled in a laminar-specific fashion. To examine specific sublaminae across the IPL, we quantified synapses across IPL depths, with 0% starting at the inner nuclear layer/inner plexiform layer (INL/IPL) border and 100% ending at the inner plexiform layer/ganglion cell layer (IPL/GCL) border. We defined the OFF sublamina, where OFF RGCs that hyperpolarize to an increase in light intensity stratify their dendrites, as 0–40% IPL depth, whereas the ON sublamina, where ON RGCs that depolarize in response to light stratify their dendrites, is defined to span 40–100% IPL depth (Figure 2A).[24,25] Across the IPL, both CtBP2 and PSD95 density decreased as a function of time, with greater synapse loss in the OFF versus ON sublamina

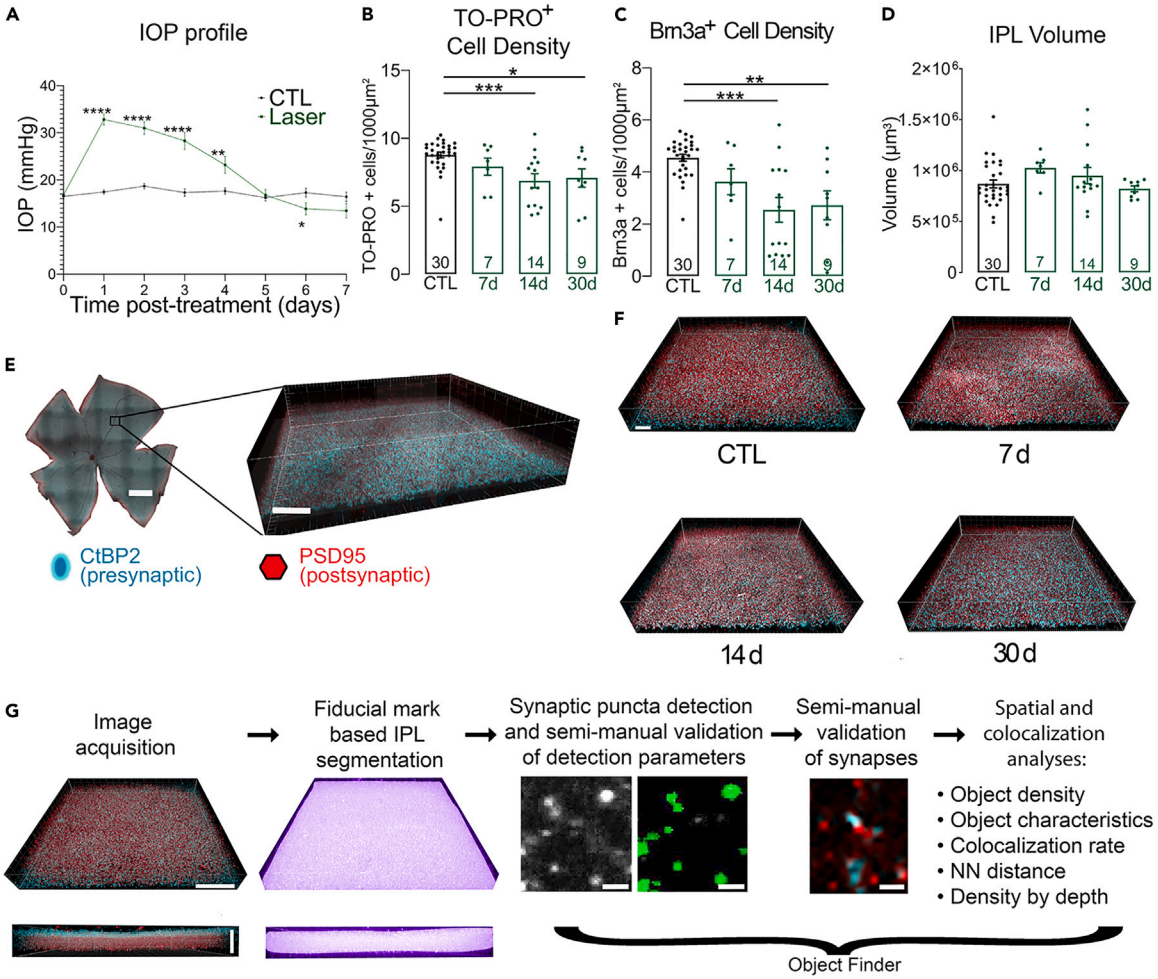
A
IOP profile
CTL
Laser
IOP (mmHg)
Time post-treatment (days)
B
TO-PRO+ Cell Density
TO-PRO + cells/1000µm²
C
Brn3a+ Cell Density
Brn3a + cells/1000µm²
D
IPL Volume
Volume (µm³)
CTL
7d
14d
30d
E
CtBP2 (presynaptic)
PSD95 (postsynaptic)
F
CTL
7d
14d
30d
G
Image acquisition
Fiducial mark based IPL segmentation
Synaptic puncta detection and semi-manual validation of detection parameters
Semi-manual validation of synapses
Spatial and colocalization analyses:
• Object density
• Object characteristics
• Colocalization rate
• NN distance
• Density by depth
Object Finder

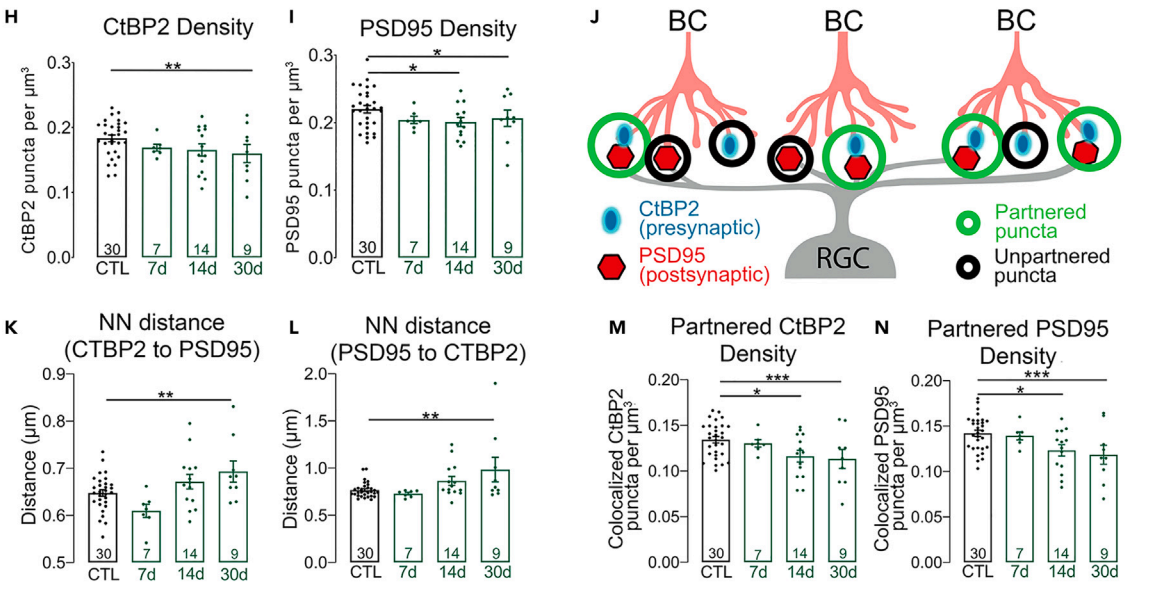
H
CtBP2 Density
CtBP2 puncta per µm³
I
PSD95 Density
PSD95 puncta per µm³
J
BC
BC
BC
CtBP2 (presynaptic)
PSD95 (postsynaptic)
RGC
Partnered puncta
Unpartnered puncta
K
NN distance (CTBP2 to PSD95)
Distance (µm)
L
NN distance (PSD95 to CTBP2)
Distance (µm)
M
Partnered CtBP2 Density
Colocalized CtBP2 puncta per µm³
N
Partnered PSD95 Density
Colocalized PSD95 puncta per µm³

Figure 1. IOP elevation results in loss of pre- and postsynaptic components throughout the inner retina

(A) IOP as a function of time after the laser-induced ocular hypertension procedure for both control (black) and laser eyes (green).

(B) Average TO-PRO-3$^+$ density in the ganglion cell layer (GCL) in control, 7, 14, and 30 days retina (Kruskal-Wallis test, p = 0.0029).

(C) Average Brn3a$^+$ density in the GCL in control, 7, 14, and 30 days retina (Kruskal-Wallis test, p = 0.0005).

(D) Average IPL volume in control, 7, 14, and 30 days retina (Kruskal-Wallis test, p = 0.0964).

(E) Image of an entire retina wholemount (montage from overlapping images acquired with a 10x objective) from a control retina immunolabeled with antibodies to presynaptic component CtBP2 (cyan) and postsynaptic component PSD95 (red) Scale bar 500 μm. Inset shows a 3D render of an IPL volume. Scale bar 30 μm.

(F) 3D rendering of representative IPL volumes from control, 7, 14, and 30 days retina immunolabeled with antibodies to CtBP2 (cyan) and PSD95 (red). Scale bar 10 μm.

(G) Synapse quantification workflow: whole IPL images were acquired, and then the IPL was segmented semi-manually using fiducial marks (see STAR Methods for more detail) Scale bar 20 μm. Initial parameters for synaptic puncta detection by iterative thresholding were manually validated (raw signal in grayscale, detected puncta in green). Following, synaptic colocalization analysis parameters were manually validated before final colocalization and spatial analyses (cyan: pre, red: post). ObjectFinder was used for puncta detection, semi-manual validation, colocalization, and spatial analyses. Scale bar 2 μm.

(H) CtBP2 density (Mixed-effects analysis, p = 0.0049).

(I) PSD95 density (Mixed-effects analysis, p = 0.0259).

(J) Cartoon showing bipolar terminals with CtBP2 (cyan) colocalizing with PSD95 (red) on ganglion cell dendrites. Green circles show partnered synaptic puncta and black circles show unpartnered synaptic puncta.

(K) Average distance between CtBP2 and nearest neighboring PSD95 (Mixed-effects analysis, p = 0.0049).

(L) Average distance between PSD95 and nearest neighboring CtBP2 (Mixed-effects analysis, p = 0.0109).

(M) Partnered CtBP2 puncta density (Mixed-effects analysis, p = 0.0015).

(N) Partnered PSD95 puncta density (Mixed-effects analysis, p = 0.0008). Plots show mean ± SEM. N (animals) is shown inside histograms. Circles: individual values. Benjamini, Krieger and Yekutieli post-hoc comparisons: *<0.05, **<0.01, ***<0.001, ****<0.0001.

(Figures 2B–2E). This was especially apparent for PSD95, where there was significant loss of postsynaptic components in the OFF sublamina at 14 and 30 days after IOP elevation (PSD95 density by IPL depth integral mean ± SD: ON sublamina: CTL:100.±14.32, 7 days:92.84 ± 10.17, 14 days:92.5 ± 11.69, 30 days:94.78 ± 15.51, Mixed-effects model, p = 0.1/OFF sublamina: CTL:100 ± 14.2, 7 days: 86.24 ± 11.11, 14 days:88.4 ± 14.34, 30 days: 92.79 ± 18.38, Mixed-effects model, p = 0.005). In the ON sublamina, only presynaptic component CtBP2 was lost 30 days after IOP elevation, while PSD95 density remained relatively stable in the ON sublamina (CtBP2 density by IPL depth integral mean ± SD: ON sublamina: CTL:100.±14.14, 7 days:90.68 ± 11.76, 14 days:92.07 ± 15.56, 30 days:92.66 ± 14.69, Mixed-effects model, p = 0.01/OFF sublamina: CTL:100 ± 23.39, 7 days: 88.95 ± 14.66, 14 days:86.79 ± 30.09, 30 days:79.04 ± 41.26, Mixed-effects model, p = 0.007).

Loss of partnered synaptic components is asymmetric between pre- and postsynaptic sites

During retinal synapse assembly in development, partnered synaptic components are more stable than unpartnered synaptic components,[26] i.e., presynaptic components colocalized to a postsynaptic component, or vice versa, are more stable than synaptic components that are not colocalized to a partner. Therefore, we wondered whether partnered or unpartnered synaptic components are more resilient or vulnerable during synapse disassembly in neurodegeneration, and we examined this from the perspective of the presynaptic component (CtBP2 as reference object) and from the perspective of the postsynaptic component (PSD95 as reference object) (Figure 3A). Early after IOP elevation at 7 days, unpartnered CtBP2 and unpartnered PSD95 showed a trend toward decreasing (only the decrease of unpartnered CtBP2 in the ON sublamina was statistically significant) (Figures 3G and 3I). However, by 30 days after IOP elevation, partnered CtBP2 and partnered PSD95 decreased (Figures 3B–3E; Partnered PSD95 by IPL depth integral, percentage of control mean ± SD: ON sublamina: CTL:100.0 ± 13.10, 7 days:96.77 ± 11.18, 14 days:89.04 ± 14.20, 30 days:88.54 ± 15.98, Mixed-effects model, p = 0.007/OFF sublamina: CTL:100.0 ± 19.70, 7 days: 92.42 ± 13.27, 14 days, 81.49 ± 25.37, 30 days:74.74 ± 35.82, Mixed-effects model, p = 0.0008) (Partnered CTBP2 by IPL depth integral, percentage of control mean ± SD: ON sublamina: CTL:100.0 ± 14.19, 7 days:98.21 ± 12.45, 14 days:85.34 ± 14, 30 days: 91.36 ± 12.76, Mixed-effects model, p = 0.01/OFF sublamina: CTL: 100.0 ± 17.68, 7 days: 96.82 ± 8.73, 14 days: 85.63 ± 24.17, 30 days: 79.18 ± 33.36, Mixed-effects model, p = 0.04). On the other hand, by 30 days after IOP elevation unpartnered CtBP2 and unpartnered PSD95 remained stable compared to control (Unpartnered PSD95 by IPL depth integral, percentage of control mean ± SD: ON sublamina: CTL:100.0 ± 21.47, 7 days:83.79 ± 12.61, 14 days:100.5 ± 17.10, 30 days:109.1 ± 30.17, Mixed-effects model, p = 0.64/OFF sublamina: CTL:100.0 ± 25.94, 7 days:77.93 ± 12.39, 14 days:97.70 ± 10.56, 30 days:117.1 ± 50.59, Mixed-effects model, p = 0.16). These data reflect progressive loss of partnered synaptic components as neurodegeneration progress.

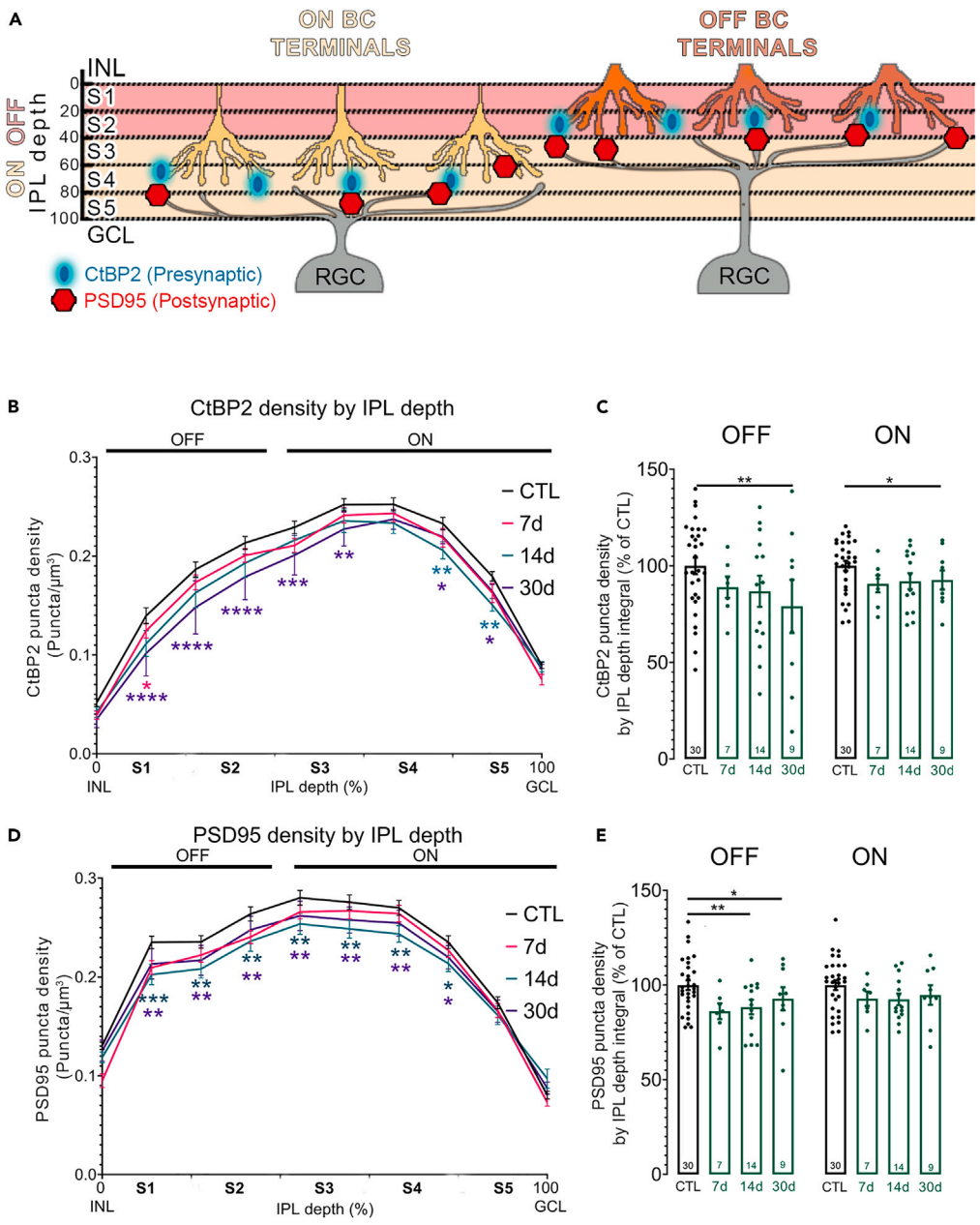

Figure 2. The pattern of synaptic component loss is sublamina-specific

(A) Cartoon showing ON and OFF BC terminals with CtBP2 (cyan) contacting PSD95 (red) at postsynaptic terminals from an OFF and an ON RGC. Lines indicate the sublaminae of the IPL (S1, S2, S3, S4, S5). Shading indicates the OFF (coral) and the ON (light yellow) sublaminae.

(B) CtBP2 density as a function of IPL depth from control (black, N = 30), 7 days (pink, N = 7), 14 days (teal, N = 14) and 30 days (purple, N = 9) (two-way mixed-effects analysis, Time $p < 0.0001$, IPL depth $p < 0.0001$).

(C) Average CtBP2 density integral in the ON and OFF sublaminae from control (black), 7, 14, and 30 days (green) (Mixed-effects analysis, ON $p = 0.01$; OFF $p = 0.007$).

(D) PSD95 density as a function of IPL depth from control (black, N = 30), 7 days (pink, N = 7), 14 days (teal, N = 14) and 30days (purple, N = 9) (2 Way Mixed-effects analysis, Time $p < 0.0001$, IPL depth $p < 0.0001$).

(E) PSD95 density integral in the ON and OFF sublaminae from control (black), 7, 14, and 30 days (green) (Mixed-effects analysis, ON $p = 0.1$; OFF $p = 0.005$). Plots show mean ± SEM. N is shown inside histograms or mentioned above. Circles: individual values. Benjamini, Krieger and Yekutieli post-hoc comparisons: *<0.05, **<0.01, ***<0.001, ****<0.0001.

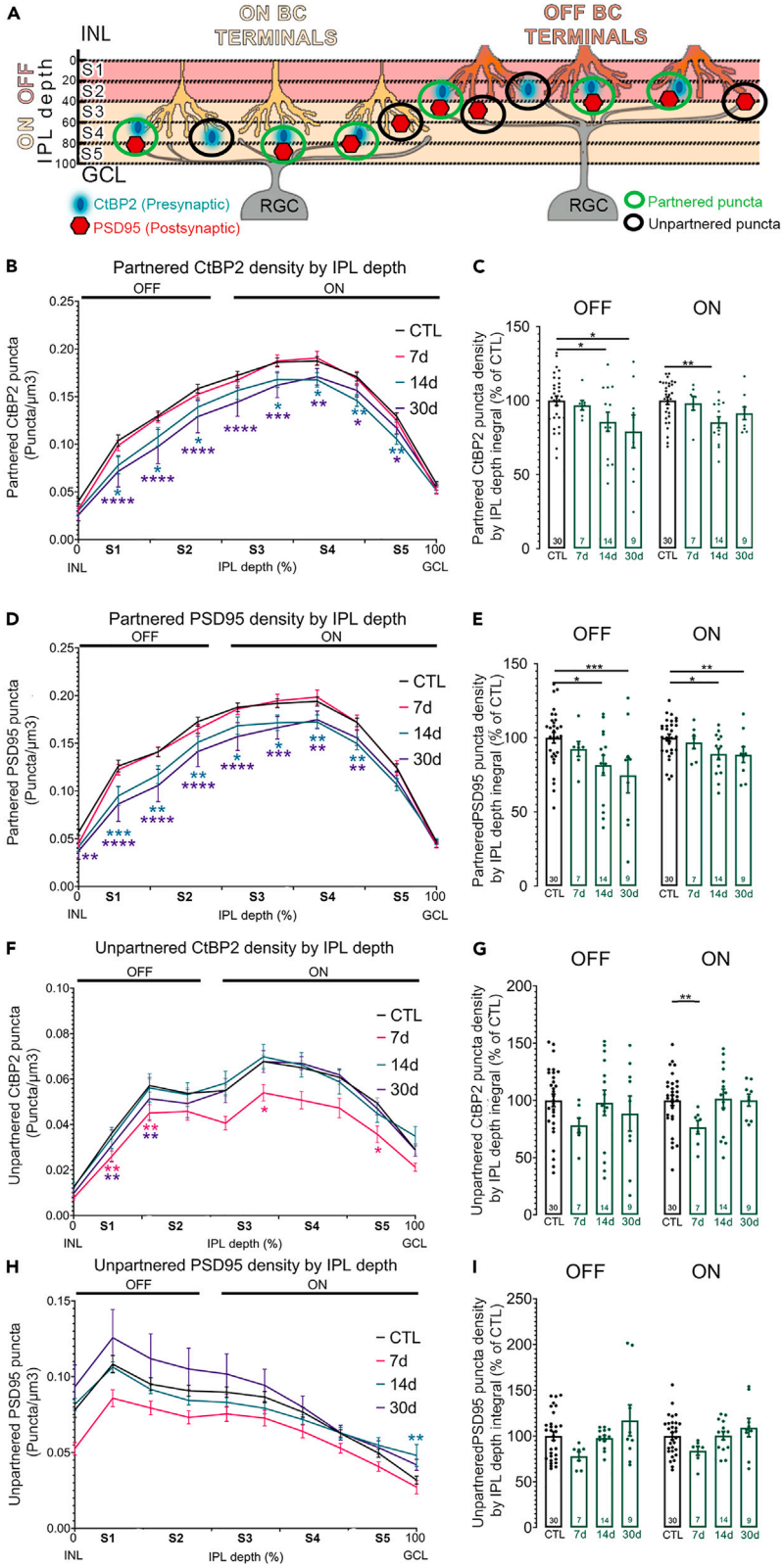
A
INL
ON BC TERMINALS
OFF BC TERMINALS
ON OFF IPL depth
S1
S2
S3
S4
S5
GCL
CtBP2 (Presynaptic)
PSD95 (Postsynaptic)
RGC
RGC
Partnered puncta
Unpartnered puncta
B
Partnered CtBP2 density by IPL depth
OFF
ON
CTL
7d
14d
30d
Partnered CtBP2 puncta (Puncta/µm3)
IPL depth (%)
INL
GCL
C
OFF
ON
Partnered CtBP2 puncta density by IPL depth inegral (% of CTL)
CTL 7d 14d 30d
D
Partnered PSD95 density by IPL depth
Partnered PSD95 puncta (Puncta/µm3)
E
PartneredPSD95 puncta density by IPL depth inegral (% of CTL)
F
Unpartnered CtBP2 density by IPL depth
Unpartnered CtBP2 puncta (Puncta/µm3)
G
Unpartnered CtBP2 puncta density by IPL depth inegral (% of CTL)
H
Unpartnered PSD95 density by IPL depth
Unpartnered PSD95 puncta (Puncta/µm3)
I
UnpartneredPSD95 puncta density by IPL depth inegral (% of CTL)

Figure 3. Loss of partnered synaptic components is asymmetric between pre- and postsynaptic sites

(A) Cartoon showing ON and OFF BC terminals with CtBP2 (cyan) contacting PSD95 (red) at postsynaptic terminals from an OFF and an ON RGC. Lines indicate the sublaminae of the IPL (S1, S2, S3, S4, S5). Shading indicates the OFF (coral) and the ON (light yellow) sublaminae. Circles show partnered (green) and unpartnered (black) synaptic puncta.

(B) Partnered CtBP2 density as a function of IPL depth from control (black, N = 30), 7 days (pink, N = 7), 14 days (teal, N = 14), and 30 days (purple, N = 9) (2 Way Mixed-effects analysis, Time $p < 0.0001$, IPL depth $p < 0.0001$).

(C) Partnered CtBP2 density integral in the ON and OFF sublaminae from control (black), 7, 14, and 30 days (green) (Mixed-effects analysis, ON $p < 0.0001$; OFF $p = 0.001$).

(D) Partnered PSD95 density as a function of IPL depth from control (black, N = 30), 7 days (pink, N = 7), 14 days (teal, N = 14), and 30 days (purple, N = 9) (2 Way Mixed-effects analysis, Time $p = 0.0002$, IPL depth $p < 0.0001$).

(E) Partnered PSD95 density integral in the ON and OFF sublaminae from control (black), 7, 14, and 30 days (green) (Mixed-effects analysis, ON $p = 0.007$; OFF $p = 0.0008$).

(F) Unpartnered CtBP2 density as a function of IPL depth from control (black, N = 30), 7 days (pink, N = 7), 14 days (teal, N = 14), and 30 days (purple, N = 9) (2 Way Mixed-effects analysis, Time $p < 0.0001$, IPL depth $p < 0.0001$).

(G) Unpartnered CtBP2 density integral in the ON and OFF sublaminae from control (black), 7, 14, and 30 days (green) (Mixed-effects analysis, ON $p = 0.04$; OFF $p = 0.03$).

(H) Unpartnered PSD95 density as a function of IPL depth from control (black, N = 30), 7 days(pink, N = 7), 14 days (teal, N = 14), and 30days (purple, N = 9) (2 Way Mixed-effects analysis, Time $p < 0.0001$, IPL depth $p < 0.0001$).

(I) Unpartnered PSD95 density integral in the ON and OFF sublaminae from control (black), 7, 14, and 30 days (green) (Mixed-effects analysis, ON $p = 0.64$; OFF $p = 0.16$). Plots show mean ± SEM. N is shown inside histograms or mentioned above. Circles: individual values. Benjamini, Krieger and Yekutieli post-hoc comparisons: *<0.05, **<0.01, ***<0.001, ****<0.0001.

Loss of presynaptic ribbons precedes or coincides with loss of postsynaptic PSD95

Next, we examined the ratio between partnered versus unpartnered synaptic components over time to evaluate the order of synapse disassembly, i.e., whether the pre- or postsynaptic component is lost first. When we examined this ratio using CtBP2 as the reference object, the ratio of partnered versus unpartnered CtBP2 remained stable over time, which is consistent with both synaptic components being lost near simultaneously (Partnered CTBP2 percentage mean ± SD: ON sublamina: CTL:73.58 ± 4.86, 7 days:77.5 ± 2.48, 14 days:70.86 ± 6.66, 30 days:70.98 ± 3.22; Mixed-effects model, $p = 0.024$, P/OFF sublamina: CTL:73.29 ± 4.38, 7 days:76.39 ± 1.98, 14 days:70.05 ± 7.01, 30 days:69.61 ± 3.63; Mixed-effects model, $p = 0.012$) (Figure 4). When we examined this ratio using PSD95 as the reference object over time, the ratio shifts toward decreased partnered PSD95 and increased unpartnered PSD95, which is consistent with the presynaptic component being lost first (Partnered PSD95 percentage mean ± SD: ON sublamina:CTL:70.07 ± 3.39,7 days:72.83 ± 3.13, 14 days:67.10 ± 5.24, 30 days:65.53 ± 6.96, Mixed-effects model, $p = 0.008$/OFF sublamina: CTL:57.39 ± 9.13,7 days:61.59 ± 3.73, 14 days:51.38 ± 9.76, 30 days:46.16 ± 19.14, Mixed-effects model, $p = 0.023$). Taken together, these findings across IPL depth suggest that presynaptic components are lost first or simultaneously with the postsynaptic component, consistent with data obtained when single ganglion cells were examined.[7]

DISCUSSION

Here, we quantified all excitatory synapses across an IPL volume of retina in the context of postsynaptic neuron degeneration. We demonstrate that after transient IOP elevation, pre- and postsynaptic components are lost throughout the IPL of the retina. Furthermore, in the ON sublamina, presynaptic components are lost, whereas in the OFF sublamina, both pre- and postsynaptic components are lost. Across the IPL, both partnered CtBP2 and partnered PSD95 are lost over time, while unpartnered CtBP2 and unpartnered PSD95 remain stable. In terms of the order of synapse disassembly, our data demonstrate either presynaptic component loss first or simultaneous loss of both pre- and postsynaptic components, which is consistent with findings uncovered when examining single RGC types.[10,12] Taken together, the results of this study underscore the generalizability of certain principles of synapse disassembly across inner retinal circuits with sublamina-specific patterns, such as more profound loss of synaptic components in the OFF sublamina. Future work is needed to determine the mechanisms underlying these patterns of synapse disassembly and potential means of recovery and restoration of synapses and circuits in adult diseased retina.

In many neurodegenerative diseases, such as Alzheimer and Parkinson's disease, synapse loss is a hallmark and indeed synapse loss serves as a prelude to major cognitive or motor decline.[27,28] In our experimental glaucoma model, ganglion cell loss occurs 14 days after IOP elevation, which is concurrent with the time point at which significant synapse loss is also identified. On the other hand, when synaptic density on

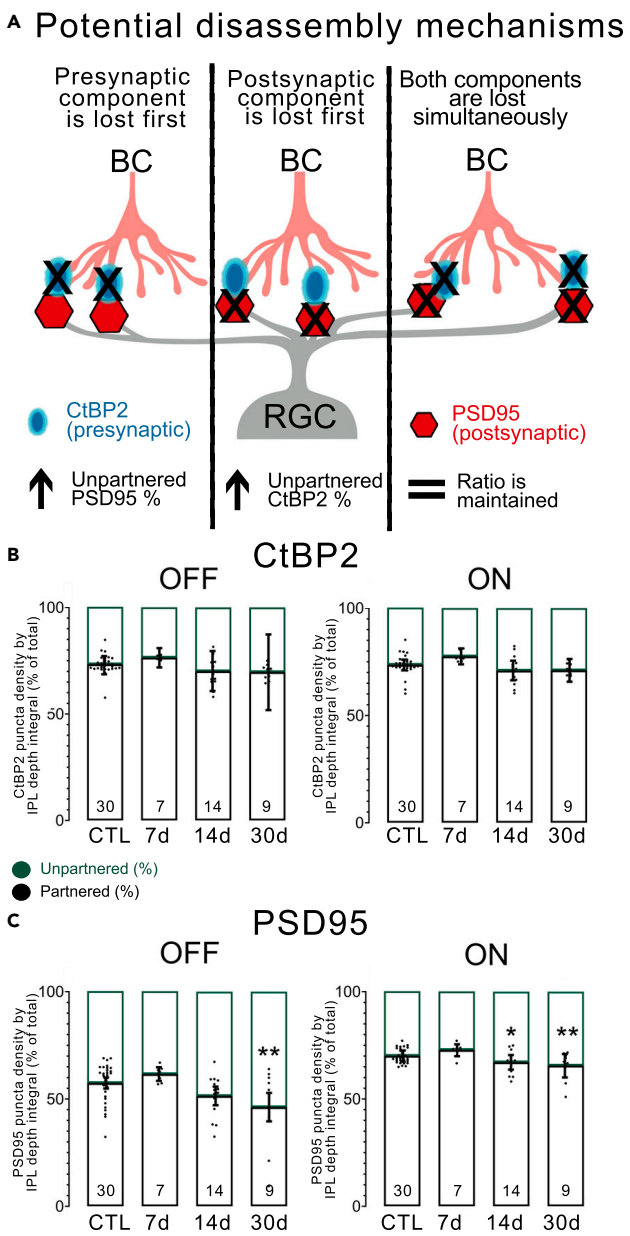

Figure 4. Loss of presynaptic ribbons precedes or coincides with loss of postsynaptic PSD95

(A) Cartoon showing BC terminals with CtBP2 (cyan) contacting PSD95 (red) at postsynaptic terminals from an RGC. Potential disassembly mechanisms with their predicted impact on the ratio between partnered versus unpartnered synaptic components: the presynaptic component is lost first (left), the postsynaptic component is lost first (center), both components are lost simultaneously (right).

(B) Partnered (black) and unpartnered (green) CtBP2 percentage for the OFF (left) and ON (right) sublaminae for control, 7, 14, and 30 days (Mixed-effects model: OFF sublamina, $p = 0.012$/ON sublamina, $p = 0.024$).

(C) Partnered (black) and (green) unpartnered PSD95 percentage for the OFF (left) and ON (right) sublaminae for control, 7, 14, and 30 days (Mixed-effects model: OFF sublamina, $p = 0.023$/ON sublamina, $p = 0.008$). Plots: show mean ± SEM. N is shown inside histograms. Circles: individual values. Benjamini, Krieger and Yekutieli post-hoc comparisons: *<0.05, **<0.01.

individual alpha ganglion cells was analyzed in the same model, synapse loss began as early as 7 days after IOP elevation.[12] While the whole IPL analysis presented here provides a more expansive view of synapse disassembly compared to the single cell analysis, it is possible that the discrepancy in timing of synapse

loss in relation to RGC death is because of the fact that this IPL analysis includes labeling of synapses other than ribbon synapses between bipolar to ganglion cell synapses.

While previous data supports the concept that ganglion cells that stratify in the OFF sublamina are more vulnerable in experimental glaucoma,[8–13] there is controversy in the field. Previous work in several different models of rodent experimental glaucoma focused on examination of specific RGC types, demonstrating that αON RGCs were as equally affected as other types such as αOFF or ON-OFF RGCs in terms of dendritic area and complexity, and light responses.[17,19] After optic nerve crush, an unbiased analysis using single cell RNA-seq demonstrated that susceptibility may not be based solely on ON versus OFF functional type,[20] although the order of susceptibility in this study of the alpha RGCs followed our previous findings.[10,12] Discrepancies in ON versus OFF susceptibility may be attributable to different magnitude and duration of IOP elevation, rodent strains, timepoints examined, or quantification techniques. In this study, we limited our analysis to glutamatergic excitatory ribbon synapses in a model of transient IOP elevation, thus further work examining conventional excitatory synapses and/or inhibitory synapses is still needed. The strength of this study is the unbiased examination of pre- and postsynaptic proteins labeled by CtBP2 and PSD95 across the IPL, which revealed that the susceptibility of pre- and postsynaptic components is sublamina-dependent. In the ON sublamina, only CtBP2 shows significant loss at 30 days after IOP elevation. However, when examining the OFF sublamina, PSD95 is lost the earliest at 14 days, with both CtBP2 and PSD95 density decreased after 30 days. Taken together, these findings are consistent with the principle that synapses in the OFF sublamina are more susceptible to loss of their components than synapses in the ON sublamina.

The possible reasons for greater synapse component susceptibility in the OFF versus ON sublamina may be because of several different etiologies. For example, if IOP elevation results in decreased synaptic output of photoreceptors, OFF bipolar cells may become less likely to depolarize while ON bipolar cells may become more likely to depolarize. This change in bipolar cell excitability could be one reason why there is greater loss of presynaptic ribbon components in the OFF sublamina. Another possibility is that OFF RGCs are more susceptible to IOP elevation, and loss of these RGCs results in greater synaptic component loss in the OFF sublamina. Finally, other cell types such as microglia or differences in vascular perfusion of different IPL sublamina may be involved in the differential susceptibility of synapses and RGCs that stratify in the OFF sublamina.[29]

The patterns of synapse disassembly in neurodegeneration do not fully recapitulate patterns observed during synapse assembly in retina development. During assembly of bipolar-ganglion cell ribbon synapses, Okawa et al. found that newly formed bipolar-ganglion cell synapses are stabilized when the pre- and postsynaptic components are colocalized, i.e., partnered.[26] During the early stages of neurodegeneration in our model at 7 days after IOP elevation (Figure 3G), unpartnered CtBP2 in the ON sublamina decreased while partnered synaptic components were more resilient, which is consistent with Okawa et al.'s findings. However, as neurodegeneration progress over time, our study demonstrates that partnered synaptic components are lost while unpartnered synaptic components remain unchanged. This is in contrast to development, during which ribbons were more stable in the IPL when apposed to PSD95, and PSD95 puncta on RGC dendrites were more stable when apposed to ribbons.[26] It is possible that this discrepancy reflects the fact that we are not following individual synapses over time but are instead examining a population of synaptic components. For example, the loss of partnered synaptic components may reflect loss of both components or loss of one component, the latter resulting in the generation of an unpartnered synaptic component. This is one potential explanation for the result that as partnered synaptic components are lost on average, unpartnered synaptic components remain unchanged over time. Future studies using time-lapse imaging of both ribbons and PSD95 are needed to definitively reveal the dynamics of synapse disassembly in neurodegeneration.

We previously demonstrated in individual $A_{ON\text{-}Sustained}$ RGC analysis that presynaptic ribbons are disassembled before postsynaptic component loss, a surprising finding given the paradigm of postsynaptic neuron injury as the initiating event in glaucoma pathogenesis.[7] Our data are consistent with the possibility that pre- and postsynaptic components are either disassembled simultaneously, or sequentially with the presynaptic side lost first. In developing hippocampus, microglia have been shown to perform selective partial phagocytosis, or trogocytosis (trogo-: nibble), of presynaptic components.[30] Indeed, microglia partially phagocytosed presynaptic components and rearranged spine head filopodia to new bouton contacts, suggesting that microglia may be mediating rearrangement of synapses from inefficient synapses to

more efficient ones. Whether the sequential synapse disassembly pattern seen in this experimental glaucoma model is mediated by microglia awaits future studies.

From the perspective of a single ganglion cell, we have previously observed synapse disassembly, input elimination, and uncoupling between bipolar inputs and the $A_{ON\text{-}Sustained}$ ganglion cells in adult diseased retina.[7] Our findings here suggest that principles governing synapse disassembly after transient IOP elevation is both sublamina and cell-type dependent, without a single pattern governing the disassembly of the entire synaptic layer of the inner retina. Although synapse and circuit assembly occur in a sublamina-specific manner during development, our data suggests that synapse disassembly during neurodegeneration also follows a sublamina-specific pattern. Determining whether synapse disassembly is a mechanism for modulating the strength of connectivity between two neurons, as well as the window of time during which synapse disassembly is occurring without major uncoupling or input elimination would be critical for developing novel neuroprotection or neuroenhancing interventions for diseases such as glaucoma. Furthermore, alpha RGCs have the capacity for insulin-mediated dendrite and synapse regeneration,[31] but sublamina differences in circuit reassembly remain unexplored. Indeed, clinical translation of these findings may be on the horizon with the application of ultrahigh resolution visible light optical coherence tomography (OCT) to image human retina, whereby IPL sublamina can now be identified,[32,33] and the relationship between IPL sublamina thickness and ganglion cell dysfunction can be examined in glaucoma patients.

Limitations of the study

We acknowledge several limitations. First, our findings are limited to this experimental glaucoma model in mouse, which induces transiently elevated IOP and may not reflect the neurodegenerative process in humans. Second, in contrast with our study, Risner et al. found in a microbead injection model that presynaptic proteins transiently increased while postsynaptic proteins were initially preserved.[19] This discrepancy, which may be because of differences in models, magnitude of IOP elevation, or method of analysis, highlights the difficulty of translating principles of synapse disassembly across models. Third, while we have localized synaptic changes at the level of glutamatergic excitatory synapses, we have not examined conventional synapses or inhibitory synapses. In addition, PSD95 immunolabeling marks excitatory postsynaptic sites on all neurons, not just ganglion cells, thus disassembly patterns identified in the current IPL dataset are not directly comparable to studies examining individual RGCs expressing PDS95.[7]

STAR★METHODS

Detailed methods are provided in the online version of this paper and include the following:

- KEY RESOURCES TABLE
- RESOURCE AVAILABILITY
  - Lead contact
  - Materials availability
  - Data and code availability
- EXPERIMENTAL MODEL AND STUDY PARTICIPANT DETAILS
  - Animals
- METHOD DETAILS
  - Laser-induced ocular hypertension
  - Immunohistochemistry
  - Image acquisition
  - Quantification of RGCs
  - Presynaptic ribbon and postsynaptic terminal density quantification
- QUANTIFICATION AND STATISTICAL ANALYSIS

ACKNOWLEDGMENTS

We thank Felice Dunn and David Copenhagen for helpful discussions and comments, and Verónica Liliana Argüello for assistance with the figures. This work was supported by the NIH-NEI (EY028148 to Y.O., EY002162 to UCSF Vison Core), E. Matilda Ziegler Foundation for the Blind (Y.O.), BrightFocus Foundation (Y.O.), NVIDIA corporation (L.D.S.), Glaucoma Research Foundation (L.D.S. and Y.O.), All May See Foundation (Y.O., L.D.S., and M.S.), and Research to Prevent Blindness (unrestricted grant to UCSF Department of Ophthalmology).

AUTHOR CONTRIBUTIONS

Conceptualization, L.D.S. and Y.O.; Methodology, L.D.S. and Y.O.; Investigation, M.S., A.K.Y., and Y.O.; Software, L.D.S.; Writing – Original Draft, M.S. and Y.O.; Writing – Review and Editing, M.S., L.D.S., and Y.O.; Funding Acquisition – M.S., L.D.S., and Y.O.; Supervision, Y.O.

DECLARATION OF INTERESTS

The authors declare no competing interests.

INCLUSION AND DIVERSITY

One or more of the authors of this paper self-identifies as an underrepresented ethnic minority in their field of research or within their geographical location. One or more authors of this paper self-identifies as a gender minority in their field of research.

Received: March 10, 2023
Revised: May 9, 2023
Accepted: June 27, 2023
Published: July 1, 2023

REFERENCES

1. Hashimoto, K., and Kano, M. (2013). Synapse elimination in the developing cerebellum. Cell. Mol. Life Sci. *70*, 4667–4680. https://doi.org/10.1007/s00018-013-1405-2.

2. Kano, M., and Watanabe, T. (2019). Developmental synapse remodeling in the cerebellum and visual thalamus. F1000Res. *8*. F1000 Faculty Rev-1191. https://doi.org/10.12688/f1000research.18903.1.

3. Luo, L., and O'Leary, D.D.M. (2005). Axon retraction and degeneration in development and disease. Annu. Rev. Neurosci. *28*, 127–156. https://doi.org/10.1146/annurev.neuro.28.061604.135632.

4. Mumm, J.S., Godinho, L., Morgan, J.L., Oakley, D.M., Schroeter, E.H., and Wong, R.O.L. (2005). Laminar circuit formation in the vertebrate retina. Prog. Brain Res. *147*, 155–169. https://doi.org/10.1016/S0079-6123(04)47012-5.

5. D'Orazi, F.D., Suzuki, S.C., and Wong, R.O. (2014). Neuronal remodeling in retinal circuit assembly, disassembly, and reassembly. Trends Neurosci. *37*, 594–603. https://doi.org/10.1016/j.tins.2014.07.009.

6. Berry, R.H., Qu, J., John, S.W.M., Howell, G.R., and Jakobs, T.C. (2015). Synapse loss and dendrite remodeling in a mouse model of glaucoma. PLoS One *10*, e0144341. https://doi.org/10.1371/journal.pone.0144341.

7. Della Santina, L., Yu, A.K., Harris, S.C., Soliño, M., Garcia Ruiz, T., Most, J., Kuo, Y.-M., Dunn, F.A., and Ou, Y. (2021). Disassembly and rewiring of a mature converging excitatory circuit following injury. Cell Rep. *36*, 109463. https://doi.org/10.1016/j.celrep.2021.109463.

8. Daniel, S., Clark, A.F., and McDowell, C.M. (2018). Subtype-specific response of retinal ganglion cells to optic nerve crush. Cell Death Dis. *4*, 7. https://doi.org/10.1038/s41420-018-0069-y.

9. Della Santina, L., and Ou, Y. (2017). Who's lost first? Susceptibility of retinal ganglion cell types in experimental glaucoma. Exp. Eye Res. *158*, 43–50. https://doi.org/10.1016/j.exer.2016.06.006.

10. Della Santina, L., Inman, D.M., Lupien, C.B., Horner, P.J., and Wong, R.O.L. (2013). Differential progression of structural and functional alterations in distinct retinal ganglion cell types in a mouse model of glaucoma. J. Neurosci. *33*, 17444–17457. https://doi.org/10.1523/JNEUROSCI.5461-12.2013.

11. El-Danaf, R.N., and Huberman, A.D. (2015). Characteristic patterns of dendritic remodeling in early-stage glaucoma: evidence from genetically identified retinal ganglion cell types. J. Neurosci. *35*, 2329–2343. https://doi.org/10.1523/JNEUROSCI.1419-14.2015.

12. Ou, Y., Jo, R.E., Ullian, E.M., Wong, R.O.L., and Della Santina, L. (2016). Selective vulnerability of specific retinal ganglion cell types and synapses after transient ocular hypertension. J. Neurosci. *36*, 9240–9252. https://doi.org/10.1523/JNEUROSCI.0940-16.2016.

13. Puyang, Z., Gong, H.-Q., He, S.-G., Troy, J.B., Liu, X., and Liang, P.-J. (2017). Different functional susceptibilities of mouse retinal ganglion cell subtypes to optic nerve crush injury. Exp. Eye Res. *162*, 97–103. https://doi.org/10.1016/j.exer.2017.06.014.

14. Christensen, I., Lu, B., Yang, N., Huang, K., Wang, P., and Tian, N. (2019). The susceptibility of retinal ganglion cells to glutamatergic excitotoxicity is type-specific. Front. Neurosci. *13*, 219. https://doi.org/10.3389/fnins.2019.00219.

15. Cone, F.E., Gelman, S.E., Son, J.L., Pease, M.E., and Quigley, H.A. (2010). Differential susceptibility to experimental glaucoma among 3 mouse strains using bead and viscoelastic injection. Exp. Eye Res. *91*, 415–424. https://doi.org/10.1016/j.exer.2010.06.018.

16. Daniel, S., Meyer, K.J., Clark, A.F., Anderson, M.G., and McDowell, C.M. (2019). Effect of ocular hypertension on the pattern of retinal ganglion cell subtype loss in a mouse model of early-onset glaucoma. Exp. Eye Res. *185*, 107703. https://doi.org/10.1016/j.exer.2019.107703.

17. Feng, L., Zhao, Y., Yoshida, M., Chen, H., Yang, J.F., Kim, T.S., Cang, J., Troy, J.B., and Liu, X. (2013). Sustained ocular hypertension induces dendritic degeneration of mouse retinal ganglion cells that depends on cell type and location. Invest. Ophthalmol. Vis. Sci. *54*, 1106–1117. https://doi.org/10.1167/iovs.12-10791.

18. Gao, J., Griner, E.M., Liu, M., Moy, J., Provencio, I., and Liu, X. (2022). Differential effects of experimental glaucoma on intrinsically photosensitive retinal ganglion cells in mice. J. Comp. Neurol. *530*, 1494–1506. https://doi.org/10.1002/cne.25293.

19. Risner, M.L., Pasini, S., Cooper, M.L., Lambert, W.S., and Calkins, D.J. (2018). Axogenic mechanism enhances retinal ganglion cell excitability during early progression in glaucoma. Proc. Natl. Acad. Sci. USA *115*, E2393–E2402. https://doi.org/10.1073/pnas.1714888115.

20. Tran, N.M., Shekhar, K., Whitney, I.E., Jacobi, A., Benhar, I., Hong, G., Yan, W., Adiconis, X., Arnold, M.E., Lee, J.M., et al. (2019). Single-cell profiles of retinal ganglion cells differing in resilience to injury reveal neuroprotective genes. Neuron *104*, 1039–1055.e12. https://doi.org/10.1016/j.neuron.2019.11.006.

21. VanderWall, K.B., Lu, B., Alfaro, J.S., Allsop, A.R., Carr, A.S., Wang, S., and Meyer, J.S. (2020). Differential susceptibility of retinal ganglion cell subtypes in acute and chronic models of injury and disease. Sci. Rep. *10*, 17359. https://doi.org/10.1038/s41598-020-71460-6.

22. Fu, C.T., and Sretavan, D. (2010). Laser-induced ocular hypertension in albino CD-1 mice. Invest. Ophthalmol. Vis. Sci. *51*, 980–990. https://doi.org/10.1167/iovs.09-4324.

23. Salinas-Navarro, M., Alarcón-Martínez, L., Valiente-Soriano, F.J., Ortín-Martínez, A., Jiménez-López, M., Avilés-Trigueros, M., Villegas-Pérez, M.P., de la Villa, P., and Vidal-Sanz, M. (2009). Functional and morphological effects of laser-induced ocular hypertension in retinas of adult albino Swiss mice. Mol. Vis. *15*, 2578–2598.

24. Famiglietti, E.V., and Kolb, H. (1976). Structural basis for ON-and OFF-center responses in retinal ganglion cells. Science *194*, 193–195. https://doi.org/10.1126/science.959847.

25. Menger, N., Pow, D.V., and Wässle, H. (1998). Glycinergic amacrine cells of the rat retina. J. Comp. Neurol. *401*, 34–46. https://doi.org/10.1002/(sici)1096-9861(19981109)401:1<34::aid-cne3>3.0.co;2-p.

26. Okawa, H., Yu, W.-Q., Matti, U., Schwarz, K., Odermatt, B., Zhong, H., Tsukamoto, Y., Lagnado, L., Rieke, F., Schmitz, F., and Wong, R.O.L. (2019). Dynamic assembly of ribbon synapses and circuit maintenance in a vertebrate sensory system. Nat. Commun. *10*, 2167. https://doi.org/10.1038/s41467-019-10123-1.

27. Picconi, B., Piccoli, G., and Calabresi, P. (2012). Synaptic dysfunction in Parkinson's disease. In Synaptic Plasticity: Dynamics, Development and Disease Advances in Experimental Medicine and Biology, M.R. Kreutz and C. Sala, eds. (Springer), pp. 553–572. https://doi.org/10.1007/978-3-7091-0932-8_24.

28. Selkoe, D.J. (2002). Alzheimer's disease is a synaptic failure. Science *298*, 789–791. https://doi.org/10.1126/science.1074069.

29. Pitale, P.M., Shen, G., Sigireddi, R.R., Polo-Prieto, M., Park, Y.H., Gibson, S.E., Westenskow, P.D., Channa, R., and Frankfort, B.J. (2022). Selective vulnerability of the intermediate retinal capillary plexus precedes retinal ganglion cell loss in ocular hypertension. Front. Cell. Neurosci. *16*, 1073786. https://doi.org/10.3389/fncel.2022.1073786.

30. Weinhard, L., di Bartolomei, G., Bolasco, G., Machado, P., Schieber, N.L., Neniskyte, U., Exiga, M., Vadisiute, A., Raggioli, A., Schertel, A., et al. (2018). Microglia remodel synapses by presynaptic trogocytosis and spine head filopodia induction. Nat. Commun. *9*, 1228. https://doi.org/10.1038/s41467-018-03566-5.

31. Agostinone, J., Alarcon-Martinez, L., Gamlin, C., Yu, W.-Q., Wong, R.O.L., and Di Polo, A. (2018). Insulin signalling promotes dendrite and synapse regeneration and restores circuit function after axonal injury. Brain *141*, 1963–1980. https://doi.org/10.1093/brain/awy142.

32. Ghassabi, Z., Kuranov, R.V., Schuman, J.S., Zambrano, R., Wu, M., Liu, M., Tayebi, B., Wang, Y., Rubinoff, I., Liu, X., et al. (2022). In vivo sublayer analysis of human retinal inner plexiform layer obtained by visible-light optical coherence tomography. Invest. Ophthalmol. Vis. Sci. *63*, 18. https://doi.org/10.1167/iovs.63.1.18.

33. Zhang, T., Kho, A.M., and Srinivasan, V.J. (2021). In vivo Morphometry of Inner Plexiform Layer (IPL) stratification in the human retina with visible light optical coherence tomography. Front. Cell. Neurosci. *15*, 655096. https://doi.org/10.3389/fncel.2021.655096.

34. Kikinis, R., Pieper, S.D., and Vosburgh, K.G. (2014). 3D slicer: a platform for subject-specific image analysis, visualization, and clinical support. In Intraoperative Imaging and Image-Guided Therapy, F.A. Jolesz, ed. (Springer New York), pp. 277–289. https://doi.org/10.1007/978-1-4614-7657-3_19.

STAR★METHODS

KEY RESOURCES TABLE

REAGENT or RESOURCE	SOURCE	IDENTIFIER
Antibodies		
anti-CtBP2 mouse monoclonal antibody	BD Biosciences	Cat #612044; RRID:AB_399431
anti-PSD95 mouse monoclonal antibody	Neuromab	Cat #73-028; RRID:AB_10698024
anti-Brn3a mouse monoclonal antibody	Santa Cruz	Cat #sc-8429; RRID:AB_626765
Deposited data		
Data from this study	N/A	Zenodo Data: https://doi.org/10.5281/zenodo.7506579
Experimental models: Organisms/strains		
CD-1 albino mice (Crl:CD1(ICR) Outbred)	Charles River Laboratories	RRID: IMSR_CRL:022
Software and algorithms		
MATLAB	MathWorks	RRID:SCR_001622
VolumeCut	GitHub: https://github.com/lucadellasantina/VolumeCut	
ObjectFinder	GitHub: https://github.com/lucadellasantina/ObjectFinder	
ImageJ	NIH	RRID:SCR_003070

RESOURCE AVAILABILITY

Lead contact

Further information and requests for resources and reagents should be directed to and will be fulfilled by Yvonne Ou (yvonne.ou@ucsf.edu).

Materials availability

The study did not generate new unique reagents.

Data and code availability

- All individual numerical values that underlie the summary data displayed in the figures have been publicly deposited online (Zenodo Data: https://doi.org/10.5281/zenodo.7506579).
- All original code has been deposited at GitHub: https://github.com/lucadellasantina and is publicly available as of the date of publication. DOIs are listed in the key resources table.
- Any additional information required to reanalyze the data reported in this paper is available from the lead contact upon request.

EXPERIMENTAL MODEL AND STUDY PARTICIPANT DETAILS

Animals

CD-1 albino mice were purchased from Charles River Laboratories and were housed in animal facilities at the University of California, San Francisco, exposed to a daily light cycle of 12 h dark and 12 h light. All experiments were conducted in male and female animals 2–3 months of age. All animal procedures were approved by the Institutional Animal Care and Use Committees at University of California, San Francisco.

METHOD DETAILS

Laser-induced ocular hypertension

We induced ocular hypertension using our previously established model (Della Santina et al. 2021, Ou et al. 2016; Salinas-Navarro et al., 2009; Fu and Sretavan, 2010). Briefly, mice were anesthetized with ketamine-xylazine and IOP measured for each eye using the Tonolab rebound tonometer (Colonial Medical Supply). The probe was triggered with a custom foot pedal to minimize movement of the instrument during IOP measurement. Three measurements (each an average of 6 readings) were taken. For the laser procedure, mice were placed under a surgical microscope and an endoprobe attached to a diode laser (532 nm; Lumenis) was used to photocoagulate the limbal and at least 3–6 episcleral vessels in the left eye (300 mW laser power, 0.5 s duration, 100 μm diameter spot size) sparing the nasal aspect and the long posterior ciliary arteries. This procedure leads to the transient obstruction of aqueous outflow. After surgery, lubricant ophthalmic ointment was applied to the operative eye. Each animal received only one laser photocoagulation treatment with the untreated contralateral eye serving as the control. IOP was monitored for 7 days and mice that demonstrated at least 30% increase in IOP followed by a decline to baseline by day 7 were included in the study, whereas mice that developed an IOP >50 mmHg were excluded. Mice with overt signs of corneal edema, hyphema, and inflammation were sacrificed and excluded from the study. All lasered eyes exhibited IOP elevation, although some (~15%) did not demonstrate at least a 30% IOP increase and were not included in the study. However, it was not possible to design a control in which the eye was lasered but the IOP was not increased, and thus the contralateral untreated eye served as a control. Animals included in the study were assigned to the timepoints of interest 7days (N = 7), 14days (N = 14), 30days (N = 9) after recovering to baseline IOP (7 days after the laser procedure).

Immunohistochemistry

To visualize RGCs, nuclei, pre- and postsynaptic sites, whole-mount retinas were harvested. On the corresponding date of sacrifice, eyes were removed and placed in oxygenated mouse ACSF, containing the following (in mM): 130 NaCl, 2.5 KCl, 1 MgCl2*6H2O, 2 CaCl2*2H2O, 1.25 NaHPO4, 20 glucose, 21 NaHCO3. Retinas were isolated from the eyecup under a dissection microscope and mounted onto nitrocellulose filter paper (Millipore). Retinas were then fixed in 2% PFA in ACSF, pH 7.4, for 20–30 min. After fixation, retinas were rinsed twice in 1× PBS and processed for immunostaining as follows: blocked in blocking buffer containing 5% normal donkey serum, 2% BSA and 0.5% Triton X-100 in PBS overnight at 4°C followed by 4 night incubation using primary antibodies, including anti-CtBP2 (mouse IgG1 1:500, BD Transduction Labs, 612044, RRID: AB_399431), anti-PSD95 (mouse IgG2a 1:500, NeuroMAB, 75-028, RRID: AB_2292909) and anti-Brn3a (mouse IgG2b 1:500, Santa Cruz, sc-8429, RRID:AB_626765). Retinas were then washed 3 × 20 min in PBS and incubated overnight at 4°C with the corresponding secondary antibodies (Alexa , Invitrogen, 1:500; or Dylight, Jackson ImmunoResearch Laboratories, 1:500, conjugated fluorophores) and TO-PRO3 iodide to stain cell nuclei (1:1000; Invitrogen). Retinas were then washed with PBS three times and mounted onto glass slides using Vectashield (Vector).

Image acquisition

All images were acquired with a laser scanning confocal microscope (Leica SP8, Germany) at a 2048 x 2048 pixel resolution. Whole IPL image stacks containing the GCL were acquired using a 1.4 NA 63× oil objective (voxel size: 0.098× 0.098 × 0.3 μm). Retinal location was tracked, and 4 retinal locations (1 per retinal leaflet) in the mid-periphery were imaged.

Quantification of RGCs

All quantifications were done blindly on ImageJ on maximum intensity projection images that comprised the GCL alone. For Brn3a-labeled RGCs, images were binarized, segmented by watershed, and counted using the analyze particles tool. In the case of TO-PRO-3, a geometry to distance transformation was used, then local maximas were used to create a putative selection of nuclei that was corrected manually (non-neuron-like nuclei were excluded from the counts). Cell density was expressed as the average number of cells per image acquisition area.

Presynaptic ribbon and postsynaptic terminal density quantification

To determine CtBP2 and PSD95 puncta distribution within an IPL volume, 12-bit image stacks were acquired at 0.098 × 0.098 × 0.3 μm, sampling an IPL volume with a superficial area of 204.51 × 204.51 μm. ImageJ was used

to median filter the images to remove thermal noise. For each data point, 4 independent IPL volumes from each retinal leaflet (nasal, temporal, dorsal and ventral mid-periphery) were measured and averaged.

To define and quantify the IPL volume in each stack, we created a binary mask of the IPL with 3D Slicer[34] using the CtBP2 signal to define it. We chose CtBP2 signal as guide because it stains puncta in the IPL as well as nuclei in the GCL and INL, thereby defining the borders of the IPL.

We quantified synaptic puncta using ObjectFinder (GitHub: https://lucadellasantina.github.io/ObjectFinder/), a 3D iterative thresholding algorithm. Briefly, volumetric images are divided into smaller volumes to allow for parallel computing. In each sub-volume, the software defines the background as the most common gray value. Any voxel above the local background threshold will be detected as a candidate object. This process is repeated on each plane of the sub-volume. After iterative thresholding, segmented objects are divided by watershed. Lastly, the final set of detected objects is scored by inter-plane coherence (voxel blobs that are present in multiple z-planes will have higher score). Detected objects were validated by visually comparing them with the raw signal of the original image. A potential synapse was defined as all voxels of the object whose intensity was greater than half intensity of its peak. The average density of puncta is the total number of puncta identified in the IPL volume divided by the volume size (defined by the IPL masks). The local PSD95 and CtBP2 densities were calculated as a function of IPL depth, dividing the volume in 10 sublaminae with 0% representing the location of the INL/IPL border and 100% representing the GCL. All analyses were performed in a blinded fashion.

We also used ObjectFinder to study the spatial relationship of pre and postsynaptic puncta in the IPL. To test ObjectFinder's capacity to detect overlap between pre- and postsynaptic puncta, we compared its results with that of manual colocalization performed by 3 trained observers. We manually defined colocalization of objects in 5 sub volumes (15 × 15 μm) of the acquired IPL stacks. In all cases, the software outperformed researchers, showing that it was more stringent than its human counterparts. After this check, we defined synapses as the colocalization of pre- and postsynaptic puncta. Since ObjectFinder is more stringent than humans to detect colocalization, we chose 1% of volume overlap detected by the software as the threshold to define colocalized objects. All colocalization analyses were performed twice, once using the detected CtBP2 as anchor point (presynaptic perspective) and a second time using PSD95 (postsynaptic perspective). Mean and local densities of synapses were calculated as described above.

QUANTIFICATION AND STATISTICAL ANALYSIS

Unless otherwise stated, all measurements were reported as mean ± SEM. Analyses were performed using Kruskal-Wallis tests, mixed effects model analyses, simple linear regression and Benjamini, Krieger and Yekutieli tests for post-hoc comparisons. p values are reported as decimal numbers rounded to the second significant digit, with significance defined as p value <0.05. Number of retinas/animals are reported in each figure at the base of bar plots or in the figure legend for all other types of plots. Statistical analyses were computed using GraphPad Prism (San Diego, CA).